Highly Reversible Sn-Co Alloy Anode Using Porous Cu Foam Substrate for Li-Ion Batteries

Do-Hwan Nam, Ryoung-Hee Kim, Cho-Long Lee and Hyuk-Sang Kwon

J. Electrochem. Soc. 2012, Volume 159, Issue 11, Pages A1822-A1826.
doi: 10.1149/2.050211jes

Journal of The Electrochemical Society, **159** (11) A1822-A1826 (2012)
0013-4651/2012/159(11)/A1822/5/$28.00 © The Electrochemical Society

Highly Reversible Sn-Co Alloy Anode Using Porous Cu Foam Substrate for Li-Ion Batteries

Do-Hwan Nam, Ryoung-Hee Kim, Cho-Long Lee, and Hyuk-Sang Kwon*,z

Department of Materials Science and Engineering, Korea Advanced Institute of Science and Technology, Daejeon, Korea

A three-dimensional Sn-Co alloy electrode is prepared on porous Cu foam by electrodeposition, and its electrochemical properties are investigated by galvanostatic charge/discharge tests. The effects of the Cu foam substrate and Co alloying on the morphological and phase structural changes with cycles are examined by ex situ SEM observation and XRD analysis. The Sn-Co alloy electrode exhibits an outstanding cyclic performance with a high coulombic efficiency compared with the electrochemical performance of a pure Sn electrode deposited on a smooth Cu sheet. Ex situ SEM analysis reveals that the porous Cu foam not only inhibits the pulverization and delamination of the Sn-Co alloy from the substrate by enhancing the bond between them, but also accommodates the volumetric expansion of the active phase. Moreover, the nonequilibrium $CoSn_2$ phase formed on the Cu foam substrate reversibly reacts with Li without structural deterioration, and hence remains unchanged for 50 cycles.
 [DOI: 10.1149/2.050211jes]

Manuscript submitted May 2, 2012; revised manuscript received July 12, 2012. Published September 6, 2012. This was Paper 218 presented at the Seattle, Washington, Meeting of the Society, May 6–10, 2012.

With an increasing demand on advanced power sources with higher capacity and higher energy density compared to conventional batteries, research for new electrode materials for Li-ion batteries has become more intense. Currently, graphite anodes are insufficient to meet the needs of high-capacity batteries because of their low theoretical capacity of 372 mAh g^{-1}. Among the various alternative materials for graphite, Sn has been considered to be very attractive anode material due to its high theoretical capacity of 991 mAh g^{-1}.[1–6] However, pure Sn anode has not been put to practical use because of its poor cycle stability originating from the significant volumetric changes (up to approximately 360%) that occurs during alloying/dealloying with Li.[1] The pulverization of Sn anode caused by the volume change during cycling may produce failures in electrical contacts between Sn and current collector, thereby reducing the cyclic performance.[3–6]

To overcome the problem of Sn anode, two different approaches have been adopted by numerous research groups. One approach introduces inactive phases such as Ni,[7,8] Cu[9–12] and Co[13–23] to act as a buffer matrix against the volumetric change of the active phase. The other approach uses porous substrates that offer vacant volume to accommodate the volumetric expansion of active materials and also enhance the bond between the active materials and the current collector.[16,24–27] Both strategies have demonstrated to be effective in improving the cyclic stability of the electrode.

In a recent communication, we reported a new type of three-dimensional porous Cu foam composed of grape-like nanodeposits[28] that showed high porosity, enlarged surface area, and improved mechanical properties compared with previous foam structures.[16,25,29] When the porous Cu foam was used as substrate for Sn anode, the Cu foam accommodated the volumetric expansion of Sn and effectively inhibited the delamination of the active materials, and hence the cyclic performance of Sn anode was considerably improved.[30] Despite the effects of Cu foam, however, the gradual degradation of reversible capacity caused by the structural failure of Sn was unresolved. Accordingly, to obtain the better cyclic performance, Sn-Co alloy which exhibits high specific capacity and good cycle stability[14–18] was electrodeposited on the porous Cu foam substrate. Alloying Co with Sn reduces the absolute volume expansion of Sn by forming the buffer matrix of Co nanoparticles during the Li insertion process, and it also stabilizes the liberated Sn atoms after the Li extraction process.[13] In particular, some Sn-Co intermetallic phases such as $CoSn_2$ and $CoSn_3$ exhibit relatively high charge/discharge capacity as Li-rich phases are formed; on the other hand, Co_3Sn_2 and CoSn show small capacity due to the incomplete alloying reaction of Sn with Li.[23]

Therefore, the objective of this work is to fabricate the Sn-Co alloy electrode using the highly porous Cu foam as substrate and to examine the electrochemical properties of such electrode for Li-ion batteries anode. To evaluate the effects of Co alloying and the Cu foam substrate on the cyclic stability of a Sn-Co alloy electrode, the electrochemical characteristics of the Sn-Co alloy were investigated and compared with those of the pure Sn electrode deposited on a smooth Cu sheet. The morphological and phase structural changes of both electrodes with the cycles were studied by ex situ SEM observation and XRD analysis.

Experimental

A three-dimensional porous Cu foam was fabricated by electrodeposition at a constant current density of −3 A cm^{-2} for 4 s in a Cu sulfate electrolytic bath containing 0.2 M $CuSO_4$, 0.7 M H_2SO_4, 1.2 M $(NH_4)_2SO_4$ and 0.4 mM BTA(benzotriazole).[28] The electrodeposition was conducted using a two-electrode cell: a nodule-type Cu sheet was used as the cathode, and a Cu plate was used as the anode. The distance between the cathode and the anode was 3 cm, and the bath solution was stirred magnetically at 800 rpm and at room temperature (25°C). After the foam substrate was prepared, the Sn-Co alloy was electrodeposited on the porous Cu foam at a constant current density of −40 mA cm^{-2} for 2 min in an electrolytic bath containing 40 g L^{-1} $SnCl_2$, 17.8 g L^{-1} $CoCl_2$, 44.6 g L^{-1} $Na_4P_2O_7$, 10 g L^{-1} glycine, and 29.8 g L^{-1} NH_4OH. The electrodeposition was performed using a standard three-electrode cell with the Cu foam as the working electrode, a Pt mesh as the counter electrode, and a saturated calomel electrode (SCE, 0.241 V vs. SHE) as the reference electrode. The solution temperature was maintained at 55°C.

A pure Sn electrode was prepared on a smooth Cu sheet in a Sn pyrophosphate bath containing 30 g L^{-1} $Sn_2P_2O_7$, 120 g L^{-1} $K_4P_2O_7$ and 0.15 g L^{-1} of PEG (polyethylene glycol). The electrodeposition of Sn was executed in a two-electrode cell that consists of a smooth Cu sheet as the cathode and a Sn plate as the anode. A constant current density of −10 mA cm^{-2} was applied for 4 min at room temperature.

The electrochemical properties of the Sn-Co alloy electrode and the pure Sn electrode were investigated using 2016 coin-type cells assembled in an Ar-filled glove box. The cell is composed of a sheet of the Sn-Co alloy electrode or the pure Sn electrode (with an area of 1 cm^2), a Li metal electrode (with an area of 1 cm^2), and electrolyte containing 1 M $LiPF_6$ dissolved in EC:DMC (1:1 volume ratio). The charge/discharge characteristics of the electrode were galvanostatically examined at a current density of 100 mA g^{-1} between 0.02 V and 1.0 V (vs. Li/Li^+) at 30°C.

The surface morphology and phase structure of the electrodes were examined by scanning electron microscopy (SEM) and X-ray

*Electrochemical Society Active Member.
zE-mail: hskwon@kaist.ac.kr

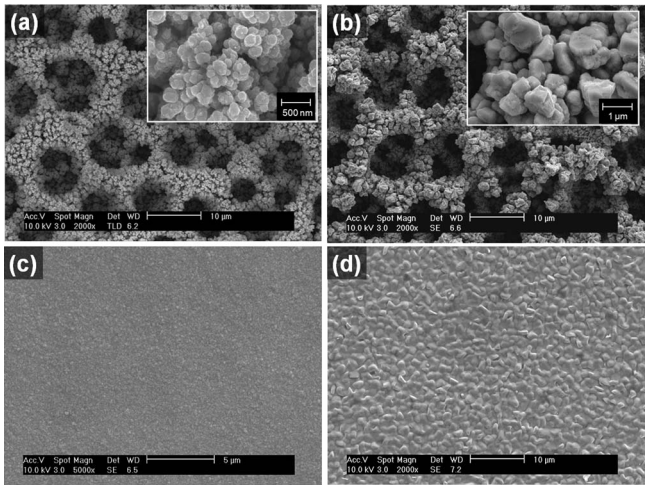

Figure 1. SEM images of (a) the porous Cu foam prepared by electrodeposition, (b) Sn-Co alloy deposited on the Cu foam, (c) the smooth Cu sheet, and (d) Sn deposited on the smooth Cu sheet.

diffraction (XRD), respectively. The composition of the electrodes was characterized by energy dispersive spectroscopy (EDS). To investigate the changes in morphology and phase structure of the electrode with cycling, ex situ SEM observation and XRD analysis were performed on each electrode.

Results and Discussion

Preparation of the Sn-Co/Cu foam electrode and the Sn/smooth Cu sheet electrode.— To clearly examine the effects of the Cu foam substrate and Co alloying on the electrochemical performance of the Sn-Co alloy electrode, two different electrodes were prepared; a Sn-Co alloy electrode deposited on Cu foam, and a pure Sn electrode deposited on a smooth Cu sheet.

Fig. 1 shows the SEM images of (a) the Cu foam, (b) the Sn-Co alloy deposited on the Cu foam, (c) the smooth Cu sheet, and (d) Sn deposited on the smooth Cu sheet. As shown in Fig. 1a, the Cu foam prepared by electrodeposition exhibits a three-dimensional porous structure with compact foam walls that consist of grape-like Cu nanostructures.[28] The Cu foam also shows a smaller pore size and larger surface area than those reported previously.[16,25,29] Fig. 1b demonstrates that the Sn-Co alloy is uniformly deposited along the surface of the Cu deposits; thus, the Sn-Co alloy electrode also exhibits a three-dimensional porous structure with a large surface area, similar to the structure of the Cu foam. On the other hand, the surface of the smooth Cu sheet is flat with no pits or bumps (shown in Fig 1c). When the Sn was electrodeposited on the smooth Cu sheet, the morphology of the electrodes was similar to that of the smooth Cu sheet.

Microstructural characteristics of the Sn-Co alloy electrode on the Cu foam and the pure Sn electrode on the smooth Cu sheet are shown in Fig. 2. It is evident from EDS analysis in Fig. 2a that Sn and Co were successfully deposited on Cu foam substrate. The molar ratio of Sn to Co was measured to be 2.08 by EDS analysis. Further, the XRD diffraction pattern for the Sn-Co alloy, shown in Fig. 2c clearly shows

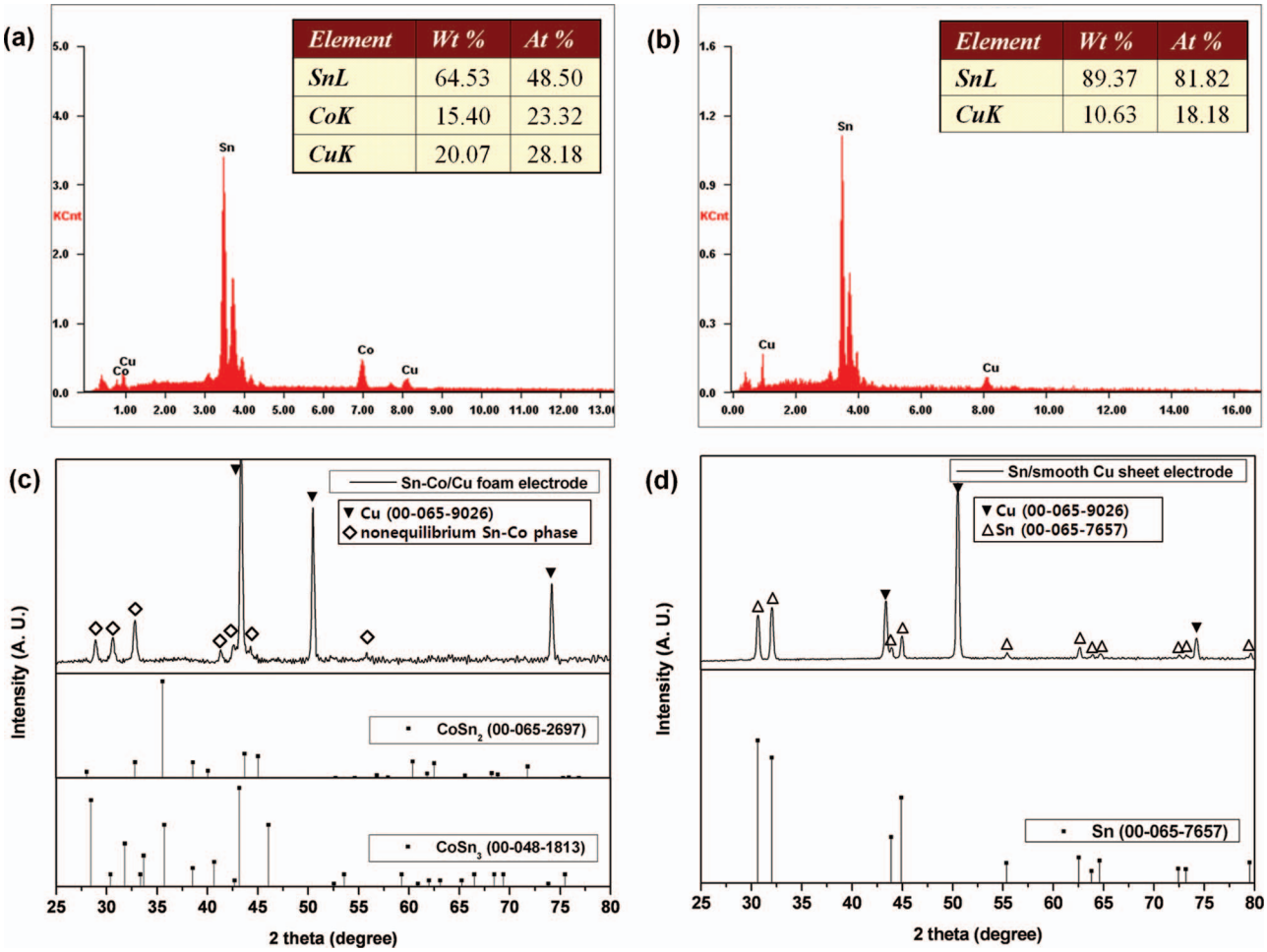

Figure 2. EDS analysis of (a) the Sn-Co electrode deposited on the Cu foam and (b) Sn electrode deposited on the smooth Cu sheet. The figure also shows the XRD patterns for (c) the Sn-Co alloy electrode deposited on the Cu foam and (d) the Sn electrode deposited on the smooth Cu sheet.

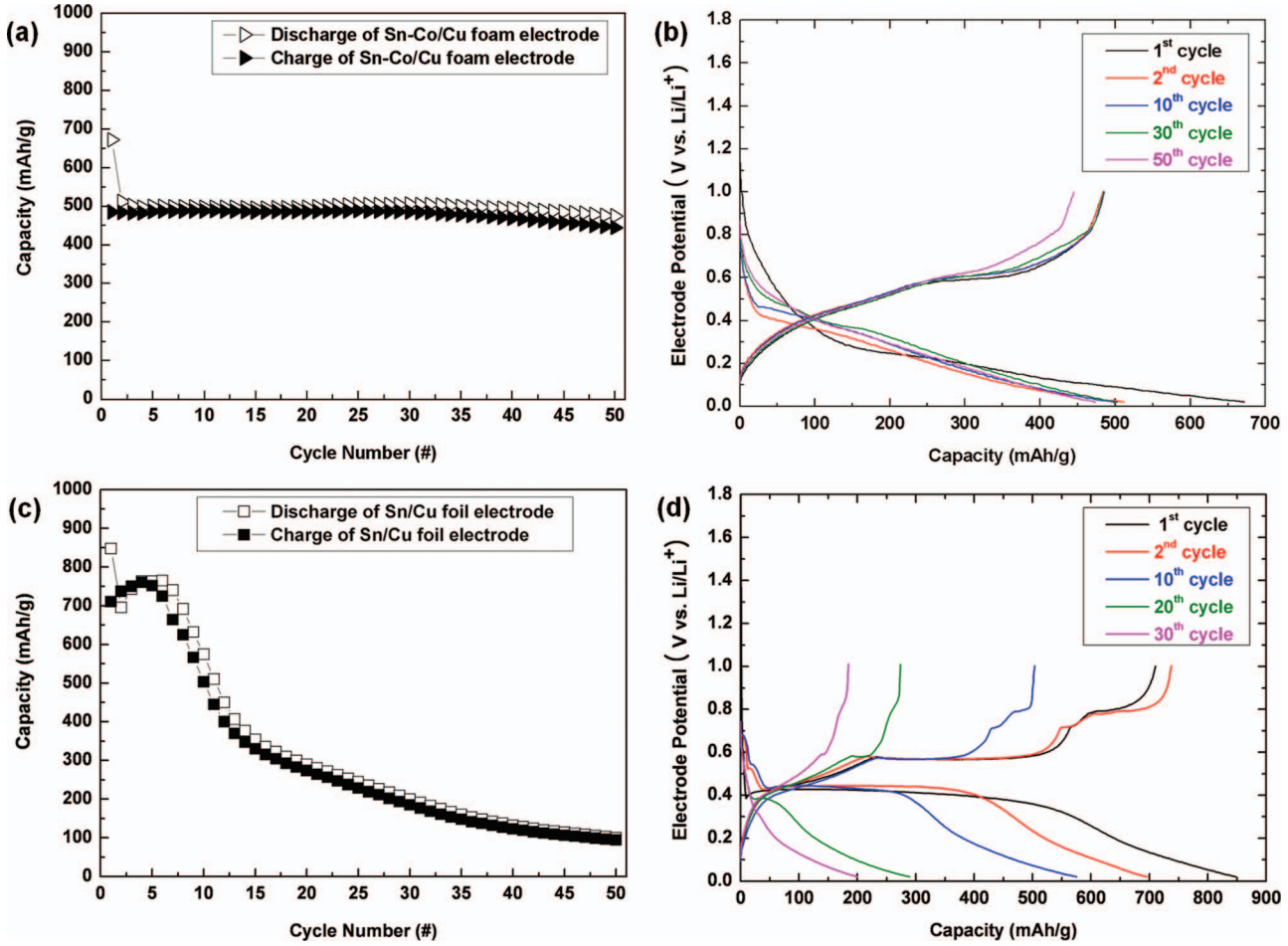

Figure 3. (a) Cyclic performance and (b) charge/discharge behavior of the Sn-Co alloy electrode deposited on the Cu foam. (c) Cyclic performance and (d) charge/discharge behavior of the Sn electrode deposited on the smooth Cu sheet. All tests were performed at galvanostatic current densities of 100 mA g^{-1} and the potential range between 0.02 and 1.0 V (vs. Li/Li^+).

the formation of nonequilibrium Sn-Co alloy phase. When compared with the reference $CoSn_3$ phase (JCPDS card No. 00-048-1813) or the reference $CoSn_2$ phase (JCPDS card No. 00-065-2697), the XRD main peaks of the Sn-Co alloy do not correspond to those of $CoSn_3$ or those of $CoSn_2$, but these are identical to the XRD pattern of the sputtered $CoSn_2$ film.[17] Based on the results of previous studies,[17,18] it could be assumed that the deposited Sn-Co alloy may be mainly composed of crystalline $CoSn_2$ and a small amount of amorphous Sn-rich phase. As shown in Fig. 2b and Fig. 2d, the EDS and XRD analysis on the Sn electrode confirm that pure Sn was successfully deposited on the smooth Cu sheet without impurities, and it matched the crystalline β-Sn phase shown in the reference β-Sn phase (JCPDS Card No. 00-065-7657).

Electrochemical properties of the Sn-Co/Cu foam electrode and the Sn/smooth Cu sheet electrode.— Fig. 3 shows cyclic performance and charge/discharge behavior of the Sn-Co alloy electrode on the Cu foam and the pure Sn electrode on the smooth Cu sheet at a constant current density of 100 mA g^{-1} between 0.02 and 1.0 V (vs. Li/Li^+). In this paper, a Li insertion into the electrode is referred to as discharge and a Li extraction as charge, based on the half-cell reaction. As illustrated in Fig. 3a, the Sn-Co alloy electrode exhibits outstanding cyclic performance, and a charge capacity is maintained at 444.7 mAh g^{-1} after 50 cycles; this corresponds to 91.8% of its initial charge capacity. Moreover, the Sn-Co alloy electrode retains high coulombic efficiency higher than 95% during 50 cycles, with the exception of the initial cycle. These results verify that the Sn-Co alloy reversibly reacted with Li with high stability, and the capacity fade caused by volumetric changes of Sn was effectively inhibited. Fig. 3b displays the charge/discharge behavior of the Sn-Co alloy electrode. In the initial cycle, the discharge and charge capacities were 671.7 mAh g^{-1} and 484.5 mAh g^{-1}, respectively, corresponding to a capacity loss of 27.8%.

During lithiation process, Li would be inserted into the Sn-Co alloy and cause the Li_xSn alloy to be formed uniformly in the Co nanoparticles according to the following equation:[19]

$$CoSn_2 + 2xLi^+ + 2xe^- \rightarrow 2Li_xSn + Co\,(x \sim 3.5) \qquad [1]$$

Ionica-Bousquet et al. demonstrated that one Sn atom would react with 3.5 Li atoms in the reaction of $CoSn_2$ with Li; thus, the estimated theoretical capacity of $CoSn_2$ is calculated to be 633 mAh g^{-1}. In Fig. 3b, however, the first charge capacity of 494.49 mAh g^{-1} was much lower than the estimated capacity of 633 mAh g^{-1}, indicating an incomplete alloying reaction of Sn; i.e., not all Sn atoms in the Sn-Co alloy reacted with Li.

In the subsequent cycles, the potential plateau assigned to the insertion of Li into the Sn-Co alloy increases from 0.25 V to 0.5 V in the 2nd cycle, and the discharge and charge curves remain almost the same behavior from the 2nd cycle to 50th cycle. Since the process of the lithiation/delithiation reactions depends on the phase structure of the electrode, the voltage profiles sustained for 50 cycles indicate that the Sn-Co alloy undergoes stable lithiation/delithiation reactions without changing its phase structure.

On the other hand, the cyclic performance of the pure Sn electrode deposited on the smooth Cu sheet was very poor. As shown in Fig. 3c, the initial charge capacity was measured to be 710.13 mAh g^{-1} with

a coulombic efficiency of 83.75%. In the following cycles, the charge capacity increased slightly to 760.82 mAh g^{-1} until the 4th cycle, but the charge capacity decreased sharply after the 5th cycle. The charge capacity of the Sn electrode faded to 94.21 mAh g^{-1} after 50 cycles, which is 13.26% of its initial charge capacity. The abrupt degradation of capacity is typical behavior for the pure Sn electrode, and this is due to the electrical isolation of Sn from the current collector caused by the pulverization associated with extreme volume changes in Sn during lithiation/delithiation.[2–6]

The charge/discharge curves of the Sn electrode were quite different from those of the Sn-Co alloy electrode. As shown in Fig. 3d, a number of potential plateaus can be observed in the discharge-charge curves that correspond to the lithiation/delithiation potentials of the Li-Sn cell.[2–5] In the 1st and 2nd cycle, the longest flat potential was observed at 0.4 V in the discharge curve and at 0.6 V in the charge curve; those plateaus are attributed to the phase transitions between LiSn and Li_7Sn_2.[5] In the subsequent cycles, however, the longest plateaus became shorter and the charge/discharge curves became round. These changes were clearly observed before and after the 10th cycle, when the discharge and charge capacities rapidly faded, indicating that the reaction process of Sn with Li was changed by factors such as the loss of the active phase or the structural changes of the active material. Consequently, the amount of Li inserted to Sn was significantly reduced.

Structural changes of the Sn-Co/Cu foam electrode and the Sn/smooth Cu sheet electrode after cycling.— Generally, the lithiation/delithiation characteristics and the reversible charge capacity of the electrode are determined by the phase structure and surface morphology of the electrode; the process of the reactions with Li depend on the structure of the active phase, and the reaction kinetics are affected by the surface area and morphology of the electrode.[18] Therefore, to explain how the electrochemical performance of the Sn-Co alloy electrode on the Cu foam improves, the changes in the electrode morphology and phase structure during the cycles were investigated, and their effects on the electrochemical properties were discussed.

Fig. 4 shows the morphological changes of the pure Sn electrode after (a) 1 cycle, (b) 5 cycles, (c) 10 cycles, and (d) 20 cycles. After the 1st cycle (Fig. 4a), a large number of cracks were generated on the electrode surface due to the volumetric expansion of Sn during the 1st discharge, and these cracks divided into much smaller islands with gaps widening between them after 5 cycles (Fig. 4b). These morphological changes enlarged the surface area and provided additional reaction sites not available with the small surface area at the 1st cycle. Therefore, the discharge capacity of the pure Sn electrode increased slightly during the first 5 cycles due to the increase in the reaction sites. After 10 cycles (Fig. 4c), however, the islands of active materials were peeled off from the smooth Cu sheet, resulting in electrical disconnection; this became more obvious after 20 cycles (Fig. 4d). Thus, it is clear that the reversible capacity of the pure Sn electrode rapidly decreased as the Sn islands were detached from the current collector with the cycles.[2–6]

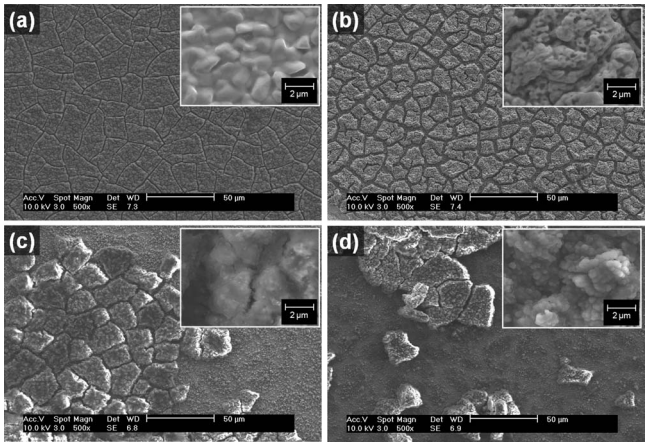

Figure 4. SEM images of the Sn electrode deposited on the smooth Cu sheet after (a) 1 cycle, (b) 5 cycles, (c) 10 cycles, and (d) 20 cycles.

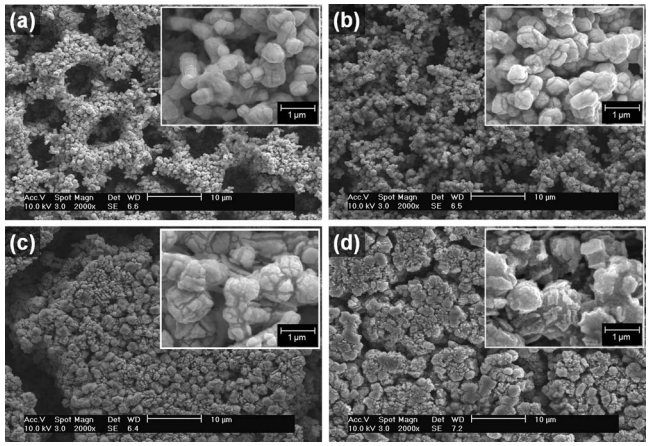

Figure 5. SEM images of the Sn-Co electrode deposited on the Cu foam after (a) 5 cycles, (b) 10 cycles, (c) 20 cycles, and (d) 40 cycles.

In contrast, the Sn-Co alloy electrode deposited on the Cu foam showed much less cracking and detachment between the active materials and the substrate with cycling. Fig. 5 shows the morphological changes of the Sn-Co alloy electrode after (a) 5 cycles, (b) 10 cycles, (c) 20 cycles, and (d) 40 cycles. As shown in Fig. 5a, the porous foam structure was maintained even after 5 cycles, indicating that the Sn-Co alloy reversibly expands and contracts without significant cracking. This is due primarily to the fact that the Cu foam with high porosity accommodates the volumetric expansion of the electrode. Even though the surface morphology of the electrode did not sustain the "foam structure" after 10 cycles, the micropores of the electrode were changed to sufficient voids that can accommodate the volumetric expansion of the active materials, resulting in the reduced internal stress and strain. Thus, active materials were not detached from the substrate during 40 cycles. A highly magnified SEM image shown in the inset of Fig. 5d confirms the presence of the pores in Sn-Co alloys even after 40 cycles.

XRD patterns for the pure Sn electrode deposited on the smooth Cu sheet with cycles are shown in Fig. 6a. Until the 5th cycle, the XRD pattern for the Sn electrode was similar to that of the as-deposited electrode, exhibiting crystalline β-Sn. However, the intensity of the main peaks assigned to β-Sn dramatically decreased after 20 cycles, which implies that β-Sn changed to a phase with lower crystallinity. Typically, an amorphization of active materials may occur in Li storage metals such as Sn and Si after a number of cycles; this is because forming a stable amorphous phase is thermodynamically more favorable than forming a crystalline phase.[31] Therefore, the decrease in the peak intensity of Sn implies that the crystalline Sn transformed into the stable amorphous Sn to reduce the free energy of the system. Accordingly, the lithiation/delithiation reactions of Sn should be modified by the change in its phase structure; this is why the charge/discharge behavior of the pure Sn electrode changed after a number of cycles (Fig. 3d). On the contrary, the phase structure of the Sn-Co alloy remained same after 50 cycles without any phase transformation. As depicted in Fig. 2c, the phase of Sn-Co alloy was characterized as the nonequilibrium $CoSn_2$ by the three main peaks around 30° and the three additional peaks at around 43°. As shown in Fig. 6b, the peak intensities were unchanged from the as-deposited electrode to the electrode after 50 cycles, confirming that the $CoSn_2$ reacted with Li without changing its phase structure. N. Tamura et al. demonstrated that the nonequlilibrium $CoSn_2$ phase which has phase structure of 92.1Sn-7.9Co can reversibly react with Li by recovering its crystal structure, because that phase is the most stable structure

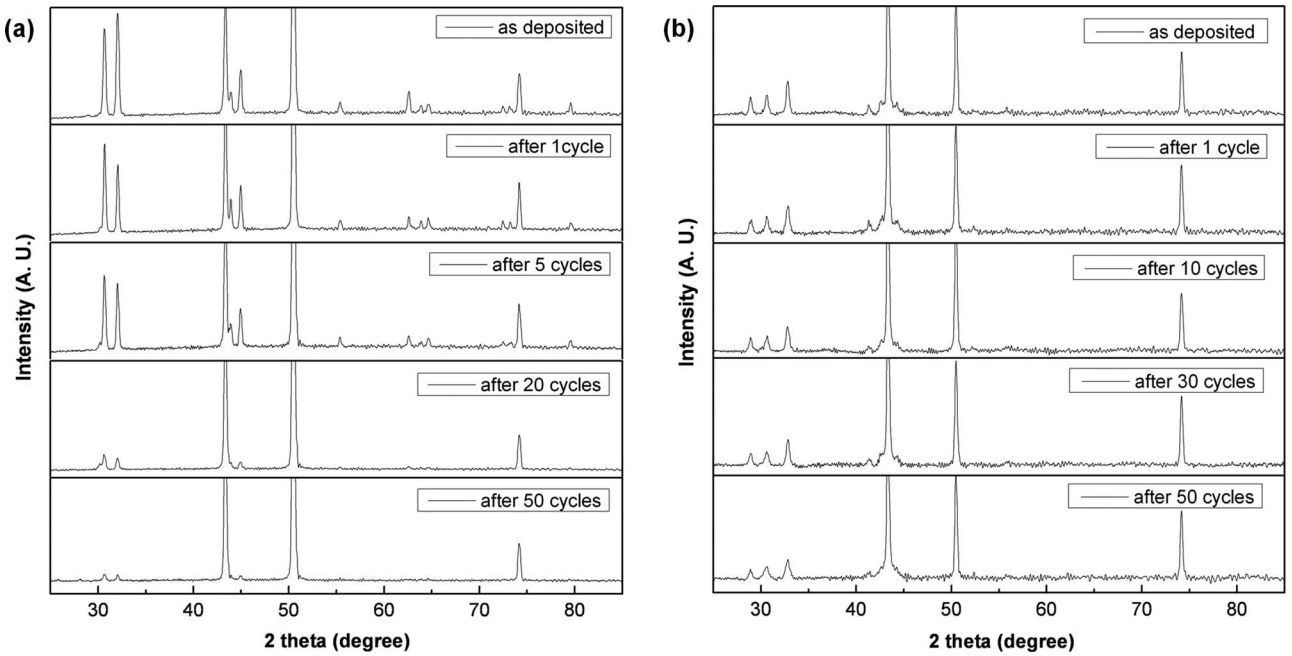

Figure 6. XRD patterns for the as-deposited electrode and the electrode after the cycles: (a) the Sn electrode on the smooth Cu sheet after 1 cycle, 5 cycles, 20 cycles and 50 cycles, and (b) Sn-Co alloy electrode on the Cu foam after 1 cycle, 10 cycles, 30 cycles and 50 cycles.

for electrochemical reaction with Li.[17] Hence, the $CoSn_2$ effectively resists to a structural deterioration due probably to its highly stable phase structure.

Conclusions

A three-dimensional Sn-Co alloy electrode was prepared by electrodeposition on the porous Cu foam, and its electrochemical properties were examined. Compared with the electrochemical performance of a pure Sn electrode deposited on a smooth Cu sheet, the Sn-Co alloy electrode on the Cu foam exhibits an improved cycle performance with a relatively high coulombic efficiency. It was confirmed from the analysis on the changes in morphology and phase structure of the Sn-Co alloy electrode with cycling that the significant improvement in the cycleability of the electrode was attributed to the following three factors: the enhanced bond between the active materials and the current collector, the high porosity in the electrode, and the high structural stability of the active phase in the reaction with Li. Ex situ SEM analysis revealed that the porous Cu foam can effectively inhibit the pulverization and delamination of the Sn-Co electrode from the substrate by enhancing the bond between the active material and current collector, and its pores accommodate the volumetric expansion of the active phase upon cycling. Concurrently, the phase structure of the nonequilibrium $CoSn_2$ remained unchanged after 50 cycles in the ex situ XRD analysis, indicating that the $CoSn_2$ reacted reversibly with Li without structural deterioration due to its high stability in phase structure.

Acknowledgments

This work was supported by the Growth Engine Technology Development Program and the BK21 program funded by the Korea Ministry of Knowledge Economy.

References

1. I. A. Courtney and J. R. Dahn, *J. Electrochem. Soc.*, **144**, 2045 (1997).
2. Y. Idota, K. Kubota, A. Matsufuji, Y. Maekawa, and T. Miyasaka, *Science*, **276**, 1395 (1997).
3. L. Y. Beaulieu, S. D. Beatiie, T. D. Hatchard, and J. R. Dahn, *J. Electrochem. Soc.*, **150**, A419 (2003).
4. J. O. Besenhard, J. Yang, and M. Winter, *J. Power Sources*, **68**, 87 (1997).
5. M. Winter and J. O. Besenhard, *Electrochim. Acta*, **45**, 31 (1999).
6. O. Mao, R. A. Dunlap, and J. R. Dahn, *J. Electrochem. Soc.*, **146**, 405 (1999).
7. N. R. Shin, Y. M. Kang, M. S. Song, D. Y. Kim, and H. S. Kwon, *J. Power sources*, **186**, 201 (2009).
8. H. Mukaibo, T. Momma, and T. Osaka, *J. Power Sources*, **146**, 457 (2006).
9. S. D Beattie and J. R. Dahn, *J. Electrochem. Soc.*, **150**, A894 (2003).
10. K. D. Kepler, J. T. Vaughey, and M. M. Thackeray, *Electrochem. Solid-state Lett.*, **2**, 307 (1999).
11. K. D. Kepler, J. T. Vaughey, and M. M. Thackeray, *J. Power Sources*, **81–82**, 383 (1999).
12. D. Larcher, L. Y. Beaulieu, D. D. MacNeil, and J. R. Dahn, *J. Electrochem. Soc.*, **147**, 1658 (2000).
13. G. F. Ortiz, R. Alcantara, I. Rodriguez, and J. L. Tirdo, *J. Electroanal. Chem.*, **605**, 98 (2007).
14. X. Y. Fan, F. S. Ke, G. Z. Wei, L. Huang, and S. G. Sun, *J. Solid State Electrochem.*, **13**, 1849 (2009).
15. J. T. Li, J. Swiatowska, A. Seyeux, L. Huang, V. Maurice, S. G. Sun, and P. Marcus, *J. Power. Sources*, **195**, 8251 (2010).
16. X. Y. Fan, F. S. ke, G. Z. wei, L. Huang, and S. G. Sun, *J. Alloys Compd.*, **476**, 70 (2009).
17. N. Tamura, Y. Kato, A. Mikami, M. Kamino, S. Matsuta, and S. Fujitani, *J. Electrochem. Soc.*, **153**, A2227 (2006).
18. N. Tamura, Y. Kato, A. Mikami, M. Kamino, S. Matsuta, and S. Fujitani, *J. Electrochem. Soc.*, **153**, A1626 (2006).
19. C. M. Ionica-Bousquet, P. E. Lippens, L. Aldon, J. Olivier-Fourcade, and J. C. Jumas, *Chem. Mater.*, **18**, 6442 (2006).
20. J. He, H. Zhao, J. Wang, J. Wang, and J. Chen, *J. Alloys compd.*, **508**, 629 (2010).
21. C. Yang, D. Zhang, Y. Zhao, Y. Lu, L. Wang, and J. B. Goodenough, *J. Power Sources*, **196**, 10673 (2011).
22. L. J. Xue, Y. F. Xu, L. Huanga, F. S. Ke, Y. He, Y. X. Wang, G. Z. Wei, J. T. Li, and S. G. Sun, *Electrochim. Acta*, **56**, 5979 (2011).
23. J. J. Zhang and Y. Y. Xia, *J. Electrochem. Soc.*, **153**, A1466 (2006).
24. R. H. Kim, D. W. Han, D. H. Nam, J. H. Kim, and H. S. Kwon, *J. Electrochem. Soc.*, **157**, D269 (2010).
25. L. Trahey, J. T. Vaughey, Harold H. Kung, and M. M. Thackeray, *J. Electrochem. Soc.*, **156**, A385 (2009).
26. T. Jiang, S. Zhang, X. Qiu, W. Zhu, and L. Chen, *J. Power Sources*, **166**, 503 (2007).
27. Z. Du, S. Zhang, T. Jiang, and Z. Bai, *Electrochim. Acta*, **55**, 3537 (2010).
28. D. H. Nam, R. H. Kim, D. W. Han, J. H. Kim, and H. S. Kwon, *Electrochim. Acta*, **56**, 9397 (2011).
29. H. C. Shin, J. Dong, and M. L. Liu, *Adv. Mater.*, **15**, 1610 (2003).
30. D. H. Nam, R. H. Kim, D. W. Han, and H. S. Kwon, *Electrochim. Acta*, **66**, 126 (2012).
31. W. J. Zhang, *J. Power Sources*, **96**, 877 (2011).